AFRL-RW-EG-TR-2013-108

AN EXAMINATION OF THE RESONANT ACOUSTIC MIXER'S FLOW FIELD

Douglas V. Nance

AFRL/RWWC
101 W. Eglin Blvd.
Eglin AFB, FL 32542-6810

DECEMBER 2013

INTERIM REPORT

AIR FORCE RESEARCH LABORATORY
MUNITIONS DIRECTORATE

■ **Air Force Materiel Command**　　■ **United States Air Force**　　■ **Eglin Air Force Base, FL 32542**

NOTICE AND SIGNATURE PAGE

AFRL-RW-EG-TR-2013-108 HAS BEEN REVIEWED AND IS APPROVED FOR PUBLICATION IN ACCORDANCE WITH ASSIGNED DISTRIBUTION STATEMENT.

FOR THE DIRECTOR:

Signed

Craig M. Ewing, DR-IV, Ph.D.
Munition Systems Effects Sciences CTC Lead
Weapon Engagement Division

Signed

Douglas V. Nance, Ph.D.
Research Scientist
AFRL/RWWC

REPORT DOCUMENTATION PAGE

The public reporting burden for this collection of information is estimated to average 1 hour per response, including the time for reviewing instructions, searching existing data sources, gathering and maintaining the data needed, and completing and reviewing the collection of information. Send comments regarding this burden estimate or any other aspect of this collection of information, including suggestions for reducing the burden, to Department of Defense, Washington Headquarters Services, Directorate for Information Operations and Reports (0704-0188), 1215 Jefferson Davis Highway, Suite 1204, Arlington, VA 22202-4302. Respondents should be aware that notwithstanding any other provision of law, no person shall be subject to any penalty for failing to comply with a collection of information if it does not display a currently valid OMB control number.
PLEASE DO NOT RETURN YOUR FORM TO THE ABOVE ADDRESS.

1. REPORT DATE *(DD-MM-YYYY)*	2. REPORT TYPE	3. DATES COVERED *(From - To)*

4. TITLE AND SUBTITLE

5a. CONTRACT NUMBER

5b. GRANT NUMBER

5c. PROGRAM ELEMENT NUMBER

6. AUTHOR(S)

5d. PROJECT NUMBER

5e. TASK NUMBER

5f. WORK UNIT NUMBER

7. PERFORMING ORGANIZATION NAME(S) AND ADDRESS(ES)

8. PERFORMING ORGANIZATION REPORT NUMBER

9. SPONSORING/MONITORING AGENCY NAME(S) AND ADDRESS(ES)

10. SPONSOR/MONITOR'S ACRONYM(S)

11. SPONSOR/MONITOR'S REPORT NUMBER(S)

12. DISTRIBUTION/AVAILABILITY STATEMENT

13. SUPPLEMENTARY NOTES

14. ABSTRACT

15. SUBJECT TERMS

16. SECURITY CLASSIFICATION OF:			17. LIMITATION OF ABSTRACT	18. NUMBER OF PAGES	19a. NAME OF RESPONSIBLE PERSON
a. REPORT	b. ABSTRACT	c. THIS PAGE			
					19b. TELEPHONE NUMBER *(Include area code)*

TABLE OF CONTENTS

Section   **Page**

LIST OF FIGURES

ACKNOWLEDGEMENTS

SUMMARY

This report details a second step made toward the high fidelity, first principles numerical simulation of the mixing for the resonant acoustic mixer. The current study addresses the mixing of two resins at higher, differing viscosities. Of interest is the time accurate vortical structure of the mixing flow field. As a matter of post-processing, the progression of eddy sizes is determined by wavenumber transformation. The computer code of choice employed in this study is LESLIE3D (Large Eddy Simulation with LInear Eddy modeling in 3 Dimensions) developed under grant by Suresh Menon at the Georgia Institute of Technology. Although LESLIE3D is not directly adapted for this problem, the code is imminently changeable. LESLIE3D has been modified to produce the acoustic excitation required for the mixer. In this case, we scale the viscosities in the transport algorithm to more closely mimic those of the actual resins. The results for a two-components mixing case are presented along with the ensuing wavenumber analysis.

1.0 INTRODUCTION

Many commercial processes involve the mixing of two or more materials. For instance, one may consider a convolution of chemical resins or the combination of a viscous liquid and a finely divided powder. For now, we regard the constituents of the mixture as non-reactive. That is to say, the components of the mixture do not react with one another as a result of mixing. There is no heat evolved while combining the ingredients. Although mixing is encountered daily in most processes in the physical world, its mechanism is not simple since it involves vorticity, molecular diffusion and, in many cases, turbulence. Vorticity and turbulence are truly dynamical processes where large scale material motion occurs. Adjacent "layers" of fluid are rolled together by rotational advection. The associated vortices may also stretch in three dimensions and distort with the surrounding fluid flow. These processes are far more effective than molecular diffusion in attaining rapid, effective mixing. We can think of the mixing process as occurring through eddies, moderately coherent fluid structures (perhaps vortices) with a particular length scale.[1] If we follow the rationale behind turbulence, mixing occurs as energy is transferred from larger eddies to those of smaller size. This transfer is referred to as an energy cascade. One may envision that two layers of adjacent fluid roll into a structure of size L. Then through fluid dynamics, this large eddy begins to break apart into smaller eddies of smaller length l. It follows that the constituents of the large eddy are then divided into pockets of smaller size in the combined fluid mass. The process of creating ever smaller eddies in this way is a realization of mixing. High shear mixing is a common implementation of this process.

High shear mixing is a very familiar to us. Generally, it involves the axial rotation of an array of metal or plastic blades through the volume of the material in question. Simple high shear mixing involves only a single axis of rotation, but more elaborate high shear mixers involve a second axis. In this case, the primary axis of rotation orbits this second axis. This arrangement forms what is known as a planetary high shear mixer, and this configuration is often used in the industrial environment. High shear mixing functions because of a basic property of viscosity. Molecular viscosity requires that there be no velocity difference between the blade surface and the fluid. The effect of this property is referred to as the "no-slip" condition – a classic, physical boundary condition admitted by the Navier-Stokes equations.[2] As a result, the fluid adjacent to the blade surface is dragged along with the blade causing shear. Shear may be thought of as a velocity gradient existing across adjacent layers of fluid. The layer of fluid at the blade surface moves at a different speed than adjacent fluid layers creating a shear layer. This often unstable layer tends to roll up with adjacent fluid layers, a phenomenon that typifies the mixing process. Repetition combines material layers over ever smaller scales making for thorough or more complete mixing. High shear mixing is effective and simple, but it does engender some deleterious side effects. The action of viscosity causes friction that dissipates mechanical energy into heat. In certain cases, the material being mixed may reach high temperatures. For energetic materials, this heating is not welcome. It is thought that the magnitude of the temperature rise during mixing may be mitigated if one avoids the generation of high shear. Resonant acoustic mixing may provide a solution to this problem.

Resonant Acoustic Mixing (RAM) is a process that employs acoustic waves, at a relatively low frequency (60 Hz), to drive the mixing process.[3] In RAM, the fluid and vessel are envisioned as a spring-mass-damper system where energy is transferred between the springs

and moving fluid masses. A condition of resonance is sought where acoustic energy from a driving source is directed into the kinetic energy of fluid eddies. The purpose of the present work is to document our continued research into the physics of RAM. The primary goal of the investigation is to determine whether or not some aspects of this process can be captured by high fidelity numerical simulation. The approach used here differs significantly from that employed by the developers of the RAM apparatus.[3] From their standpoint, the mixing process is described by the linear, second order ordinary differential equation used to describe the spring-mass-damper system familiar in the field of structural dynamics.[4] This system admits a resonance condition when it is forced at a natural frequency. In this case, motion is effectively undamped leading to large displacements. In the fluids analogy, this condition implies potent mixing action. On the other hand, our approach involves solving the Navier-Stokes equations via numerical means. Note that the Navier-Stokes equations are inherently nonlinear through the presence of advective terms for fluid motion.[1] It is difficult to see common ground between these two approaches since the RAM developers' model is entirely linear. The Navier-Stokes model certainly possesses mass and internal energy (the spring) while damping is represented though molecular viscosity. Although these properties are held in common by both models, for now, a direct correlation between them remains elusive.

The resins considered in the present study tend toward higher viscosity values and to low Reynolds number flow fields. In this case, at the smaller scales, viscous forces dominate over inertial forces. Viscous forces tend to dissipate or regularize fluid motion toward laminar flow. For this reason, turbulence is not likely to occur for high viscosity mixing, yet for analyzing the flow field, we may apply some of the techniques used for analyzing turbulent flow fields. As an example, we can cite the use of a Fourier wavenumber analysis for determining eddy sizes. Still, even at high viscosities, flow fields can possess unstable fluid motion. The purely hydrodynamic Rayleigh-Taylor and Richtmyer-Meshkov instabilities may occur.[5] These phenomena are true fluid instabilities that do not possess some of the physical features of turbulence such as randomness and intermittency.[1] Yet, these instabilities may participate in the mixing process.

In the expositions that follow, we continue our beginner's investigation of acoustic mixing. One theoretical interpretation of the acoustic mixing process invokes a natural coupling between acoustic pressure and velocity as dictated by the acoustic equations. Investigations to date have shown that the RAM does not use direct acoustic excitation to affect mixing. Rather, the RAM functions more like a shaker table. The mixing container is vibrated vertically at a frequency near 60 Hz. The vertical displacement may exceed an amplitude of one inch.[3] Whether or not the associated pressure and velocity fluctuations sensed by the fluid possess acoustic amplitudes remains unclear. Still, the RAM is said to have the ability to sense conditions of resonance and adjust the excitation accordingly. The studies shown below do use true acoustic excitation with fixed amplitude and at the fundamental frequency. The fluid dynamics are genuine as predicted by numerical solutions of the Navier-Stokes equations calculated by using the Large Eddy Simulation with LInear Eddy modeling in 3 Dimensions (LESLIE3D) multiphase physics computer program. Naturally, we employ a number of assumptions in conducting this research. The most profound assumption that we make is that LESLIE3D is multiphase physics code designed for compressible fluid flows. At face value, this assumption may seem to be very limiting, yet this code capability provides for the accurate resolution of waves, particularly acoustic waves. Secondly, constituent viscosities are scaled to

match the ratio of the actual viscosities. The actual component viscosities are very large, and some time is yet required to simulate this mixing problem with the real viscosity values. As a third assumption, we have not instituted gravity within the simulation. That work remains to be done in the days ahead. For now, our focus is on basic mixing dynamics driven by acoustic excitation along with the associated length scales. As is evidenced by the results shown later in this report, we can mimic the basic properties of RAM mixing reproducing major structures in the flow field.

2.0 METHODS, ASSUMPTIONS AND PROCEDURES

In the manner of review, sound or acoustic radiation is a longitudinal compression-rarefaction wave. In most cases, these waves travel as weak (linear) disturbances in a gas, liquid or solid material medium. Every isotropic medium at constant thermodynamic conditions has a fixed speed of sound (or celerity), and this speed is the maximum possible propagation speed for a weak or linear disturbance. Common acoustic waves retain linear character and may be superposed. In spite of their linear behavior, the propagation of sound waves in moving media is accurately modeled by the Navier-Stokes equations. These equations admit solutions for both linear and nonlinear waves for all speed regimes when the medium is modeled as a continuum. The media being mixed in the RAM consist of liquid resins, so the continuum assumption is valid. This Navier-Stokes system is solved by LESLIE3D, so we begin our theoretical discussion with a presentation of these equations.

2.1 Navier-Stokes Equations

The Navier-Stokes equations constitute a system of conservation laws for mass, momentum and energy (when expressed in homogeneous form).[6] For problems involving multiple phases (such as a dispersed phase of particles), the equations become nonhomogeneous. The dispersed phase equations are not addressed here, but since the overall research effort considers the mixing of nano-particles into resins, the dispersed phase is to be addressed in a future report. For our single phase problem, the overall system retains fully conservative. In Cartesian coordinates, the conservation of mass equation may be written as

$$\frac{\partial \rho}{\partial t} + \frac{\partial (\rho u_j)}{\partial x_j} = 0 \tag{1}$$

with the summation convention in effect. The conservation of momentum is enforced by the following equation.

$$\frac{\partial (\rho u_i)}{\partial t} + \frac{\partial (\rho u_i u_j + \delta_{ij} P - \tau_{ij})}{\partial x_j} = 0 \quad i = 1, \ldots, 3 \tag{2}$$

where the stress tensor τ_{ij} is defined as

$$\tau_{ij} = \lambda \delta_{ij} \frac{\partial u_k}{\partial x_k} + \mu \left(\frac{\partial u_i}{\partial x_j} + \frac{\partial u_j}{\partial x_i} \right) \tag{3}$$

Coefficient μ is the dynamic viscosity while λ is a parameter put forth by Stokes to represent the effect of dilatational stress.[2] This tensor conveys the rate of strain within the fluid and is a major contributor to the mixing process. By Stoke's hypothesis, this parameter (a second coefficient of viscosity) is normally taken as

4

$$\lambda = -\tfrac{2}{3}\mu \tag{4}$$

It follows that the first term in (3) is the dilatational stress while the second term is the shear stress. The conservation of energy equation is expressed in a similar form, i.e.,

$$\frac{\partial(\rho E)}{\partial t} + \frac{\partial[(\rho E + P)u_j - \tau_{ij}u_i + q_j]}{\partial x_j} = 0 \tag{5}$$

where

$$q_j = -K\frac{\partial T}{\partial x_j} \tag{6}$$

represents the components of the heat conduction vector within the fluid (Fourier's Law). In (5), we have also introduced the total energy per unit mass E, i.e.,

$$E = e + \tfrac{1}{2}u_k u_k \tag{7}$$

This system consisting of equations (1-7) is not mathematically closed. In order to achieve closure, we must add another relation, namely the equation of state. The equation of state, in most cases and for pure, single phase substances, relates the behavior of three thermodynamic variables. A frequently encountered form for gases is

$$P = P(\rho, e) \tag{8}$$

For the configurations discussed in this report, we employ a special form of (8) commonly known as the perfect gas equation of state.[7]

$$P = \rho R T \tag{9}$$

The research documented here still remains at an early stage, so (9) is applied in the calorically perfect manifestation where

$$R = C_p - C_v \tag{10}$$

$$e = C_v T \tag{11}$$

$$\gamma = {C_p}\big/{C_v} \tag{12}$$

C_p and C_v are both constant for the calorically perfect gas model.[6] For chemically reacting flow fields, a set of species equations are included within the system. The species equations may be expressed as

$$\frac{\partial(\rho Y_m)}{\partial t} + \frac{\partial[\rho Y_m (u_j + V_{jm})]}{\partial x_j} = \dot{\omega}_m \tag{13}$$

For a flow field containing N species, the mass fractions are constrained so that

$$\sum_{m=1}^{N} Y_m = 1 \tag{14}$$

The diffusion velocity components are defined as

$$V_{im} = -\frac{D_m}{Y_m}\frac{\partial Y_m}{\partial x_i} \tag{15}$$

with the constraint

$$\sum_{m=1}^{N} V_{im} = 0 \tag{16}$$

For multi-species flow fields, the internal energy has an alternative expression from that shown in (11). Based upon species enthalpies we have that

$$e = \sum_{m=1}^{N} Y_m h_m - \frac{P}{\rho} \tag{17}$$

where

$$h_m = \Delta h_{fm}^0 + \int_{T_0}^{T} C_{pm}(\tilde{T}) d\tilde{T} \tag{18}$$

Of course, the individual species' specific heat capacities, C_{pm}, may be taken as constant in order to conform to the calorically perfect gas model. The Navier-Stokes equations can be placed in a dimensionless form and characterized by the Reynolds and Prandtl dimensionless numbers (or groups).[8] For the RAM, these numbers can be calculated and applied to provide important information on the physics of the flow field.

For the RAM problem, the Reynolds number is important because of its impact on mixing. The extent of mixing is, in part, dictated by the scales of shear motion in a given flow field. The widest division of shear motion scales is encountered in turbulent flow fields, and turbulence thus provides the most efficient mixing. Yet, the level of turbulence is closely associated with the Reynolds number. For the resin mixing problem addressed here, the Reynolds number is on the order of unity. It follows that the flow field is not turbulent, and as a result, LESLIE3D can be used to simulate the problem in direct numerical simulation (DNS) mode. The transport model can be used to implement the resin viscosities.

2.2 Basics of the Numerical Method

LESLIE3D solves the Navier-Stokes equations in vector form via the MacCormack method.[9] The RAM flow field is characterized by slow advection speeds, so the MacCormack scheme is quite stable and has formal second order accuracy in space. LESLIE3D employs the finite volume method implemented on hexahedral grid cells. The explicit time stepping used by this method functions very well with the acoustic forcing boundary condition described in the next section.[10] It is through this algorithm that resonant acoustic mixing is simulated. The remaining cylindrical surfaces are treated as "no-slip" walls.[6,11] The simulations documented below are parallelized for 25 subdomains. LESLIE3D implements transport models that allow viscosity and thermal conductivity to vary with temperature. The mechanics of LESLIE3D's numerical algorithms are discussed more thoroughly in a previously published technical report.[8] To promote brevity in this exposition and to avoid redundancy, these discussions are omitted from this document.

2.3 Acoustic Forcing

The RAM mixes materials by exploiting the coupling that can occur between acoustic pressure (or velocity) fluctuations with fluctuating vorticity. Adjacent "layers" of fluid are wrapped together by fluid loops of circulation established by the rotary motion existing in vortices. Viscosity is an important contributor to this process since it makes the fluid layers "adhere" to one another. Acoustic forcing must be expressed in an algorithmic form that can be incorporated in LESLIE3D. Specifically, this algorithm is established within a solid surface boundary routine that sets ghost (or phantom) cell values for the boundary where the excitation is employed.[10] Forcing is applied as a perturbation added to main flow values of pressure and velocity. Consistent values of ghost cell density and internal energy are then calculated to complete the update. The manifestation of acoustic excitation applied for this report is described as follows. We assume that the acoustic pressure has fixed amplitude and angular frequency, i.e.,

$$P_{ac} = 0.1 P_{atm} \sin(2\pi f\, t) \tag{19}$$

In (19), the argument f is the forcing frequency in Hertz. The magnitude of pressure forcing may be adjusted by changing the "0.1" in (19) to some other value. Yet, this magnitude must be kept small to ensure that the perturbation magnitude does not exceed the acoustic level. The accompanying velocity perturbation is calculated from the equation

$$v_{ac} = \frac{P_{ac}}{\rho\, c} \tag{20}$$

where ρ and c are calculated in the flow field cell immediately adjacent to the wall.[10] The acoustic pressure perturbation is added to the flow field pressure found in the boundary adjacent flow field cell and then stored in the ghost cell. The acoustic velocity perturbation is added to the flow field velocity normal to the boundary and stored similarly. Internal and total energies for the

ghost cell are then computed as discussed in Section 2.1. In essence, this algorithm is a good representation for the situation where an acoustic wave enters the flow field at this boundary. However, RAM acoustic forcing seems more vibrational in nature. That is to say, the mixing canister is essential shaken at a frequency of about 60 Hz.[3] This condition is more difficult to represent in terms of a boundary condition algorithm since the entire container is shaken on a platform. Still, the algorithm described above is suitable for the calculations documented in this report.

2.4 Wavenumber Based Eddy Size Analysis

Whereas the inverse of time is a frequency-like quantity, the inverse of length is a wavenumber-like quantity. By Fourier transforming a time dependent signal, we achieve a representation of the signal in frequency space. It follows that we may analyze a signal or function in three-dimensional space via a similar process and obtain a representation of the function in terms of wavenumbers (inverse lengths). An individual wavenumber correlates to the inverse of a particular eddy size. In order to estimate the size range for eddies in the RAM flow field, we examine the vorticity, but not as vector-valued quantity. Rather, we analyze the enstrophy, ω^2, the square of the vorticity, an energy based property, i.e.,

$$\omega^2(x,y,z) = \vec{\omega}(x,y,z) \bullet \vec{\omega}(x,y,z) \tag{21}$$

where the vorticity has components defined by

$$\vec{\omega}(x,y,z) = \omega_x(x,y,z)\hat{i} + \omega_y(x,y,z)\hat{j} + \omega_z(x,y,z)\hat{k} \tag{22}$$

$$\omega_x = \frac{\partial w}{\partial y} - \frac{\partial y}{\partial z}; \quad \omega_y = \frac{\partial u}{\partial z} - \frac{\partial w}{\partial x}; \quad \omega_z = \frac{\partial v}{\partial x} - \frac{\partial u}{\partial y} \tag{23}$$

Naturally, u, v and w are the Cartesian components of fluid velocity defined at each point (x,y,z) in space. LESLIE3D calculates these flow properties at each time step. The wavenumber content must be extracted from the flow field at individual times by post-processing.

Wavenumber content requires that a mathematical transformation be performed upon the enstrophy function. This transformation has the same form as a Fourier transformation, but its argument is wavenumber. In lieu of simultaneously transforming along all three Cartesian coordinates, we transform individually along each of these coordinates. By doing so, we can avoid the difficulties associated with multiple numerical integrations. The mathematical equation for the transform is

$$\omega^2(k_l) = \iiint\limits_{Vol} \omega^2(x,y,z)\exp(-i\,k_l x_l)\,dx\,dy\,dz \tag{24}$$

Equation (24) may be evaluated via a single numerical summation over volume carrying the k_l as an independent parameter varying over a desired range (based upon the grid resolution).[12]

This parameter represents the components of wavenumber, i.e., $k_1 = k_x$; $k_2 = k_y$, and $k_3 = k_z$. By using the simple discrete version of (24) we can compute the wavenumber variation of enstrophy along each of the 3 axes. Organized flow structures characterized by circulation are detected by the transform and associated with a locus of wavenumbers. The inverse of the wavenumber (having extracted a factor of 2π) correlates to a measure of the eddy size. In this sense, higher wavenumbers correlate to smaller size eddies. In time, an indicator of thorough mixing is a progression of eddy sizes to higher wavenumbers along one of more axes. The results of this analysis are shown in Section 3.

2.5 Setting Up the Simulation

The geometry for the RAM is the simple cylinder shown in Figure 1. Its height and diameter are 8.602 cm. The current set of simulations is executed in parallel on 25 cores. For this problem, the research, parallel version of LESLIE3D is executed on a Thinkmate CentOS workstation equipped with a total of 8 AMD processors (64 cores). LESLIE3D is compiled by using GFORTRAN and MPICH2. At time zero, the mixer volume is divided into two portions;
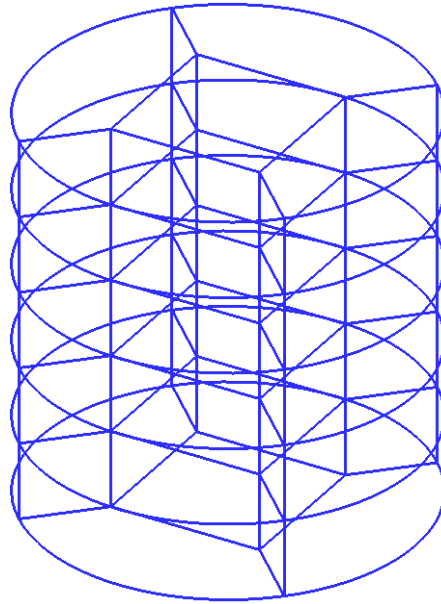

Figure 1. Grid geometry for the resonant acoustic mixer

the upper half of the RAM volume contains a simulant for resin R45-HTLO while the lower half contains a simulant for R20-LM. The best available properties for the actual resins are shown in Table 1. Properties other that molecular weight and viscosity are estimated from documentation.[13,14,15] The term simulant is used because actual viscosity values are not used for the resins. More time is required to adapt LESLIE3D for running this problem with the high viscosity values for the resins. In this case, we utilize scaled viscosity values based upon the viscosity of water vapor. As was mentioned earlier, we are building up to the genuine mixing problem by running a series of "cartoon"-like scenarios to capture basic mixing dynamics. Viscosity values in LESLIE3D's transport model are temperature dependent, but for water vapor,

the viscosity coefficients are quite small, far smaller than for resins. The approach used here is to scale the viscosity values for water vapor based upon a comparison of molecular weights for

Table 1. Thermophysical, thermochemical and transport properties for high viscosity resins

Resin	Mol. Weight (g/mol)	Viscosity (mPa.s)	Thermal Cond. (W/K/m)	C_p (J/kg/K)	Heat of Form. (J/kg/K)
R45-HTLO	2800	5000	0.1	52.63	54.40
R20-LM	1400	1400	0.1	52.63	90.67

R45-HTLO and R20-LM. The molecular weight for R54-HTLO is about 3.57 times that for R20-LM. As a result, viscosity is scaled as follows.

$$\frac{\mu H_2O}{MW\, H_2O} = \frac{\mu R20}{MW\, R20} \tag{21}$$

Based upon (21), we can show that the viscosity of simulated R20-LM should be 100 times that of water vapor. The aforementioned multiple of 3.57 is applied to scale R45 relative to R20. To summarize, simulated resin viscosity is calculated as follows.

$$\mu\, R20\text{-}LM = \mu\, H_2O\,(g) \times 100 \tag{22}$$

$$\mu\, R45\text{-}HTLO = \mu\, H_2O\,(g) \times 357 \tag{23}$$

With the use of this viscosity calculation, we see mixing occur in the simulations starting at about one second of problem time, and the ratio of resin viscosities is properly maintained.
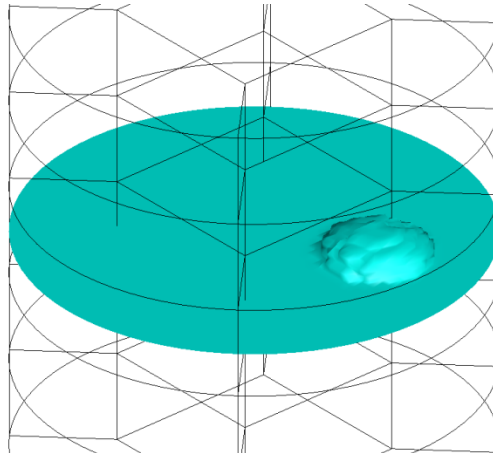
Figure 2. Perturbation placed in the interface between the two resins

Acoustic forcing is enforced at the base of the cylinder. This forcing, through the equation of state, causes temperature to elevate in the first flow cell near the base. Early on in this research, the temperature excursion caused the simulation to abort. The fix for this problem is quite simple. A heat flux condition is established at the surface to set the temperature in the ghost cells (just outside of the cylinder base) to

$$T_{Ghost\,Cell} = \tfrac{1}{2}(T_{Flow\,Cell} + 300) \tag{24}$$

Because of the symmetry inherent in the numerical model for the RAM, the process of mixing has to be, in essence, "tripped". That is to say, an asymmetric structure must be placed within the flow field to initiate shear necessary to cause rolling motion of the shear layer. For this study, we have created an off-center "dent" in the interface between the two resins. A picture of the interface is shown in Figure 2. Given the dissipative effects associated with high viscosity fluids, this perturbation is required to have a substantial magnitude, so it is easily visible in the figure, and it serves well to initiate the mixing process.

3.0 RESULTS

Since the beginning of this analysis project, LESLIE3D has been operated for over 15 million iterations for this particular RAM configuration. An average time step for the simulation is 7×10^{-7} seconds. Over 10.3 seconds of problem time have been simulated without difficulty. One datum produced by post-processing the simulations is the accelerated encountered at a point in fluid volume. We periodically record vertical velocity at a point in the fluid and then use a simple finite difference to compute acceleration. The sampling point is chosen near the base of the mixer at the location $x = -2.39$ cm; $y = 2.23$ cm; $z = 0.838$ cm. Note that the z axis is vertical for this problem. Figure 3 contains a locus of acceleration in time with the units of gravities (gees) for the sampling point. This plot is created by the instantaneous sampling of the velocity field at the monitoring point. The resulting time history is processed into an acceleration time history by finite differencing. The plot of accelerations is multimodal in that it possesses several
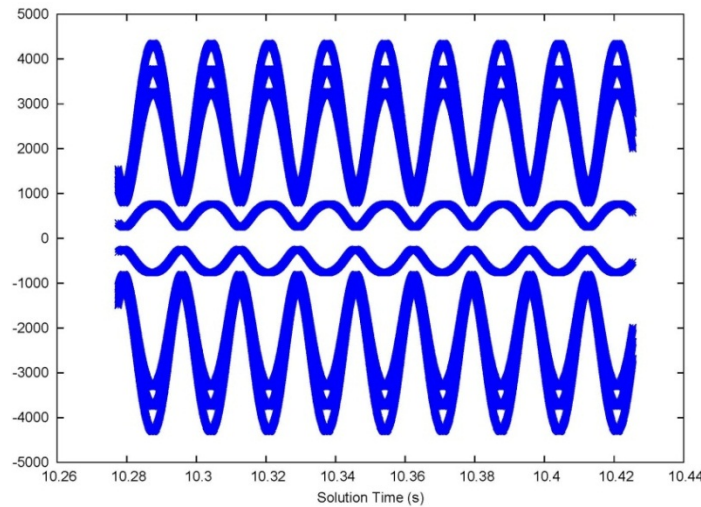

Figure 3. Fluid acceleration in gravities calculated from instantaneous velocity sampling from the numerical solution and finite differencing
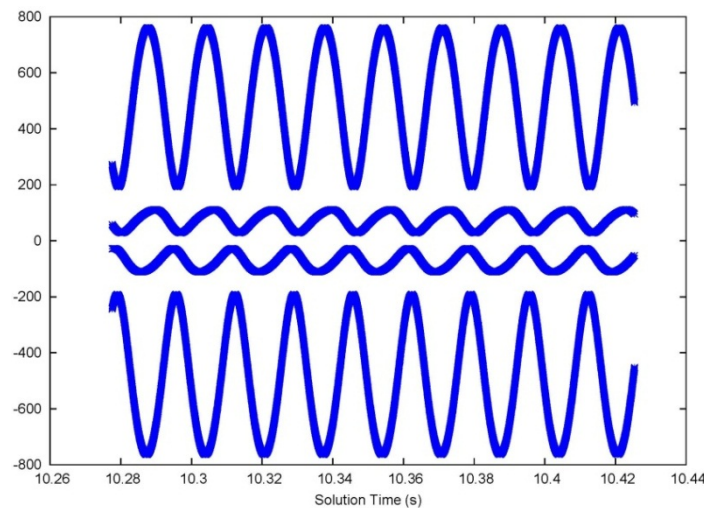

Figure 4. Fluid acceleration in gravities calculated from periodic velocity sampling from the numerical solution and finite differencing

branches with different magnitudes. The six outer limbs have ridiculously high magnitudes and are of a spurious nature. In all likelihood, these limbs are caused by numerical noise due to instantaneous sampling of the velocity field without regional averaging. The central limbs of the graph (those nearest zero) are more likely to be the true fluid accelerations. Examination of the raw acceleration data file shows that these high accelerations exist as single points with high magnitudes and even higher frequencies. As a result, they are most likely filterable, and some evidence exists to support this assertion. Consider Figure 4; in this case, the accelerations are filtered by the periodic sampling of velocities. In this case, the velocity field is sampled once every ten time steps. Note that the highest accelerations have vanished. A better procedure, reserved for future work, is to average the velocities in a neighborhood of the sampling point and eliminate the "chatter" found in the time history for a single cell in the flow field. The low magnitude limbs are still higher than the published 100 gees acceleration for the RAM, but these values are closer and match the 60 Hz frequency closely. Also, in future studies, the sampling point is to be moved further away from the acoustic source and made less subject to the effects of direct forcing.

3.1 Flow Field Structure During the Mixing Process

The LESLIE3D simulation for the RAM with two components has been temporally advanced for over 10.4 seconds of problem time. The Reynolds number for the flow field is calculated to be less than three, indicative of laminar flow. The numerical solution has been post-processed and the gross flow field structure has been examined at different snapshots in time. To illustrate the evolution of the mixing process, slices of the mass fraction field are shown. The slices are placed through the origin and are taken normal to the x and y planes. Figure 5 contains snapshots at 0.503 seconds solution time. At this time, the effect of the initial perturbation combined with acoustic excitation is to destabilize the interface. In Figure 5(a), on the constant x plane, the interface deformation looks rather uniform, but asymmetry is clearly evident on the y-plane shown in Figure 5(b). The legend for mass fraction is based upon constituent R20-LM, and as such the "hot" colors occur at the base of the RAM. It is interesting to see that although a single off-center perturbation is applied, a dual deflection has appeared in the interface. Figure
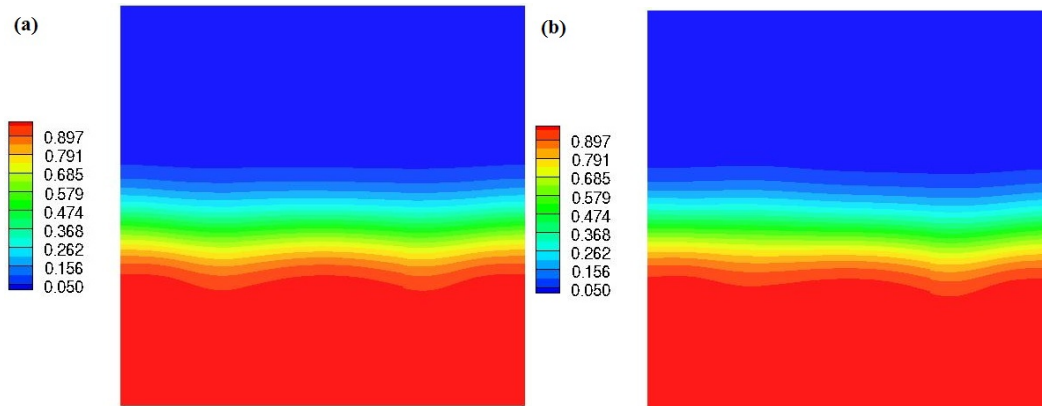

Figure 5. Contours of mass fraction for R20-LM shown (a) on the constant x-plane and (b) on the constant y-plane at 0.503 seconds problem time

Figure 6. Contours of mass fraction for R20-LM shown (a) on the constant *x*-plane and (b) on the constant *y*-plane at 1.009 seconds problem time
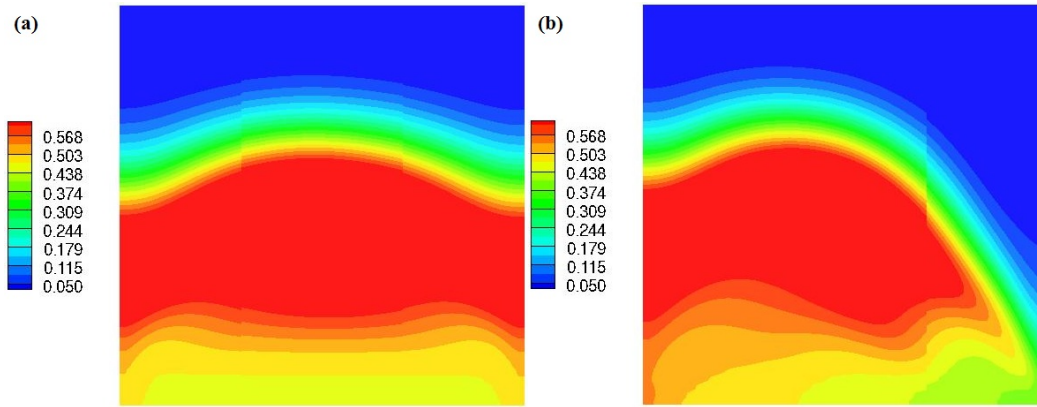
Figure 7. Contours of mass fraction for R20-LM shown (a) on the constant *x*-plane and (b) on the constant *y*-plane at 2.027 seconds problem time (scale has been reset for contour enhancement)
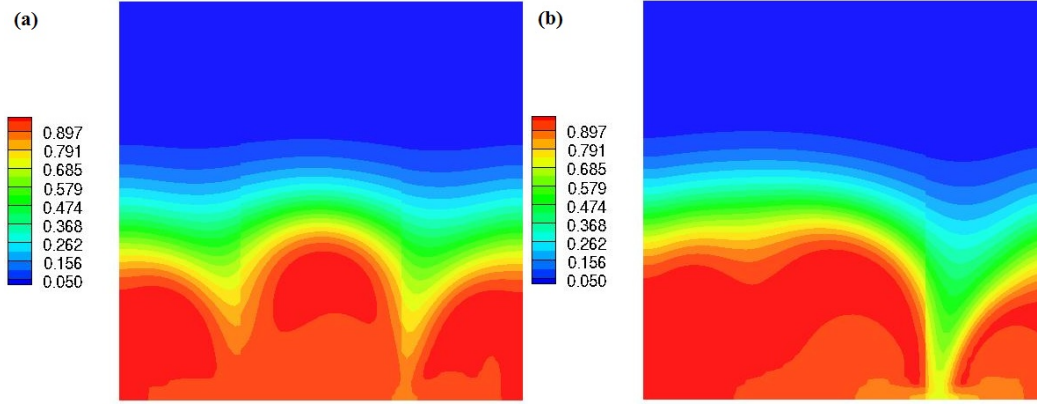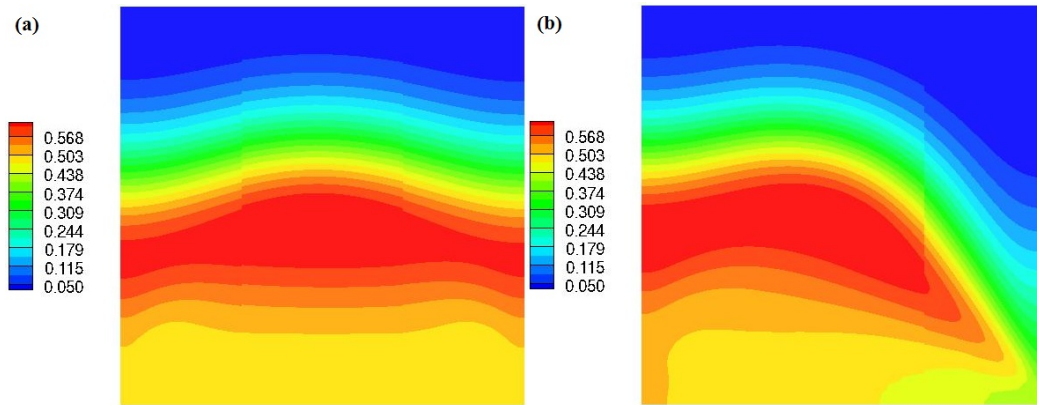

Figure 8. Contours of mass fraction for R20-LM shown (a) on the constant *x*-plane and (b) on the constant *y*-plane at 3.009 seconds problem time

6 contains similar snapshots at time 1.009 seconds. Figure 6(a) shows the less dense R20 pushing upward through the R45 resin exploiting the deflection of the interface. Along the constant *y* plane, we can see the R45 mass reaching the bottom of the RAM, so the instability is growing under acoustic excitation. Figure 7 contains mass fraction plots at 2.027 seconds; the mass

Figure 9. Iso-surface contours of R20-LM resin mass fraction shown in time sequence: (a) 0.890 s (b) 0.979 s (c) 1.130 s (d) 1.253 s (e) 1.347 s (f) 1.442 s

fraction scale has been reset in this case to make the contour more distinct. At this time, mixing is causing R-45 to infiltrate the volume near the base of the mixer. This occurren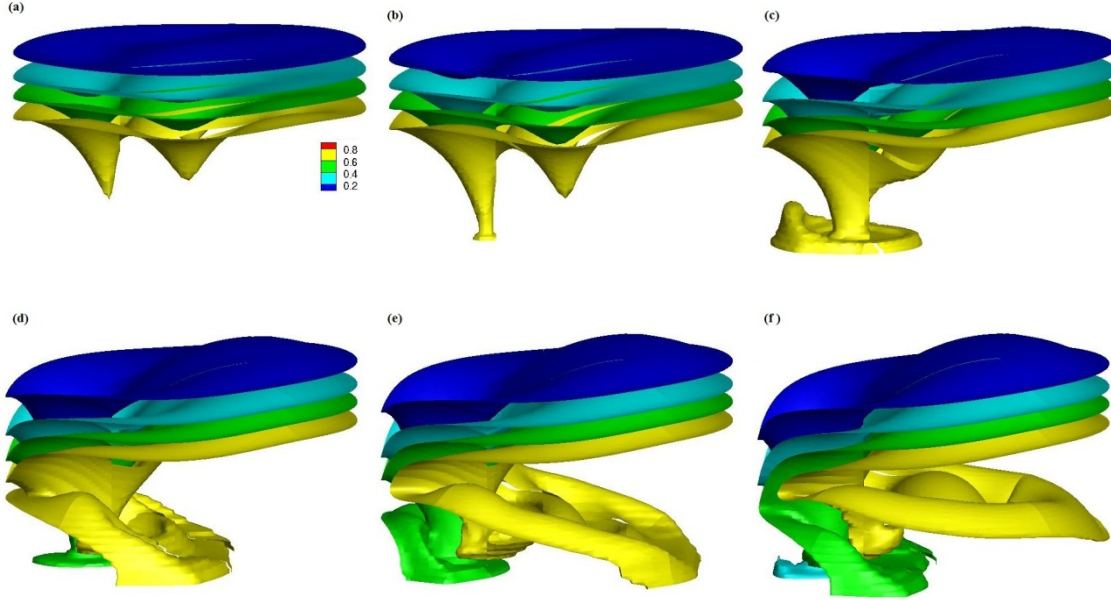ce is evidenced by the yellow color at the base of Figure 7(a). Clearly, a volume of concentrated R20 is suspended on a volume contained a greater fraction of R45. On the right side of Figure 7(b), we can see that R45 is rolling under the edge of the R20 volume. This induced flow has the effect of lifting the mass of R20 from the bottom of the mixer. In these figures, we can see the rolling together of fluid layers characteristic of shear mixing. Figure 8 contains slice plots of the mass fraction field at 3.009 seconds. The plot scale remains the same as for the previous figure. In Figure 8(a), we can see the extension of the region containing R45 build below the high concentration of R20. The region predominantly inundated by R45 is shrinking. The infiltration of R45 is even more pronounced in Figure 8(b). These findings are very interesting because the mixing is driven by the acoustic excitation, not by mechanical shear. Gravity is not implemented at this stage of the research, so R45 is not being pulled downward by gravity. In future work, the implementation of gravity is planned. Even in the plots shown, we can sense a range of scales associated with the shear flow. Note how sharply the flow turns in Figure 6(b) at the base of the mixer where the non-slip condition is satisfied. In Figures 7(b) and 8(b), we can see a range of scales at the shear interface. The finger of high concentration R20 narrows significantly near the edge of the shear near the right of the figure, and a wider vortex opens beneath the R20 that has been lifted from the mixer's base.

It is also pertinent to examine the flow field using iso-surfaces of mass fraction and vorticity. Iso-surface plots are useful in highlighting the interfaces between adjacent fluid layers containing different mass fractions of the two constituent resins. Figure 9 contains a time sequence of snapshots taken of the R20-LM mass fraction flow field. The iso-surfaces are plotted by contour level varying between 0 and 1. Note that the legend is shown in Figure 9(a). The results shown in these plots echo those shown on the slice plots but reveal three-dimensional flow structure. The same figure presents the solution at 0.890 seconds of problem time. Here we
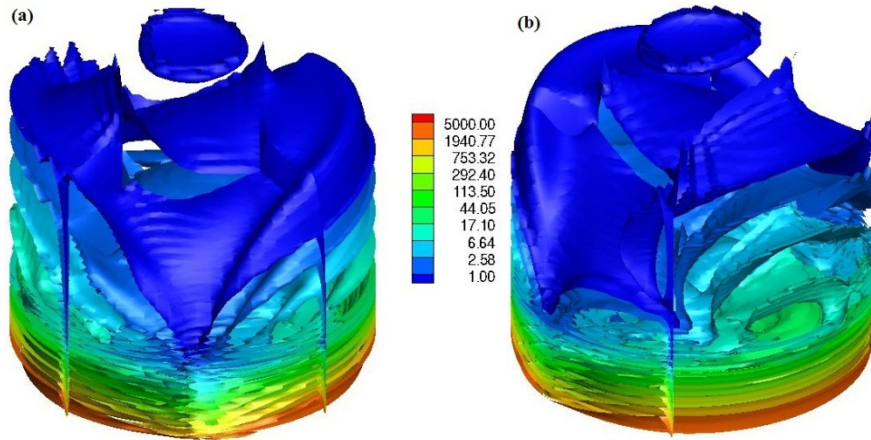
15

Figure 10. Two iso-surface views of vorticity magnitude (1/s) plotted for solution time 1.253 seconds

can see that the interface between the resins has destabilized, and R45 is beginning to infiltrate the volume of R20 from above. This effect is evidence by funnel shaped structures jutting downward. The descent of the R45 mass continues in Figure 9(b), and the leftmost structure has impacted the mixer base and begun to spread laterally. In all likelihood, these organized, funnel-shaped structures are tubes of vorticity, an assertion that is confirmed by further post-processing. In Figure 9(c), we can see that the R45 infiltrate is spreading and exerting a lifting action on the volume of concentrated R20 at 1.13 seconds. The lifting flow is also observed to interact with the mixer wall causing an excursion in the iso-surface. An interesting and somewhat new flow structure is observed in Figure 9(d). The flow is observed to roll outward in an annular ring with a core of reduced concentrate R20 pushing outward against a higher concentration annular region. In Figures 9(e) and 9(f), the core pushes forward and underneath the ring structure lifting it higher into the mixer. As a result, an entire fluid layer is pushed up into the mass of reduced concentration R20. This behavior illustrates the mixing process by the use of shear-based rolling to exchange fluid layers. The presence of vorticity may be confirmed by examining Figure 10, iso-surface plots of vorticity magnitude in the RAM. Vorticity is somewhat difficult to plot by contours since its magnitude varies so widely in the flow field. In fact, the magnitude varies through four orders of magnitude in the course of the solution. For this reason, plotting is conducted by using an exponential scale with a selective upper limit to reveal fluid structures on interest. The views shown in Figure 10 are obtained by rotating about the vertical axis. The presence of tubes of vorticity is confirmed by the presence of the layered, funnel shaped structure in Figure 10(a). Vorticity concentrates particularly at the tip of funnel and grows in magnitude for increasing radii around the vortex core. This vortex is oriented in an approximately vertical direction, and a dual vortex is similarly oriented on the opposing side of the RAM. Secondly, we can see that the flow field is rolling by examining Figure 10(b). In this case, a horizontally oriented vortex is easily observed as the cochlear shaped structure in the right foreground of this figure. This vortex is of either comparable or greater strength than the descending vortices. Note the similarity between these figures and Figure 11, a photograph made of the laboratory mixing of two resins; good agreement is observed. A final, yet no less important feature is the field of concentrated vorticity at the base of the RAM. Note that this is the locus of the most intense fluctuations in vorticity. Acoustic excitation is the cause of this phenomenon through the tight coupling between pressure fluctuations (a genuinely oscillating pressure field) and oscillating
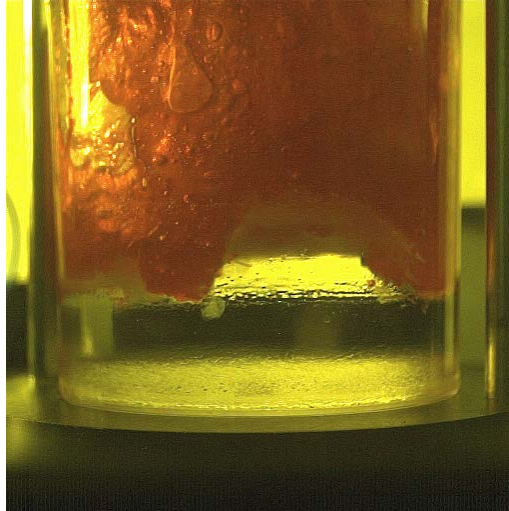
16

Figure 11. Photograph taken of a two components mixture in the RAM with descending fluid structures [Photograph by M. Bogle, Munitions Directorate, AFRL]

vorticity components.[16] Clearly, the unsteady vorticity field in this region is a driving force for continued mixing. The increasing concentration of iso-surfaces in this region strongly suggests the existence of smaller eddy sizes and a cascade of mixing scales. This issue is quantitatively examined in the next section.

3.2 Analysis of Eddy Sizes

Following the method outlined in Section 2.4, we may study the spectrum of eddy sizes for the RAM flow field by examining the directionally oriented power spectral densities of the enstrophy. These normalized spectra are developed by a space-like Fourier transformation ultimately dependent on wavenumber. Also, a spectrum can be developed for each desired Cartesian direction for individual solution snapshots in time. The approach taken here is to present x and y spectra at select solution times. Due to the long run times encountered for this problem, the z spectrum is uneventful. Figure 12 contains the x-directional spectrum at a selection of times early in the mixing process. Interestingly, the wavenumber range is populated from early in the calculation, but wavenumbers exceeding 500 m^{-1} are not trusted due to potential aliasing. What is more important is that regions of the spectrum drop in magnitude and then rebound as time advances. Also, spectral magnitudes drop for certain wavenumbers while following the baseline trend for others. While not being conclusive, this behavior is evidence for periodic energy transfers between different eddy size ranges. Figure 13 contains the y-directional enstrophy spectrum. This spectrum is more active than the x-directional spectrum in that the peak locations are less uniform and change position in time. In certain wavenumber ranges, we observe that peaks coalesce and then separate, particularly near 450 m^{-1}. This behavior is even more indicative of the transfer of energy between different sized eddies. We can also observe some flattening of the spectrum at higher wave numbers as the mixing process slowly begins to stabilize. In order to confirm these assertions, it is necessary to perform the simulation on a grid of greater density, preferably one resolved by at least a factor of two. Still, even with the presence of some aliasing in mind, the numerical solution demonstrates progressive mixing in
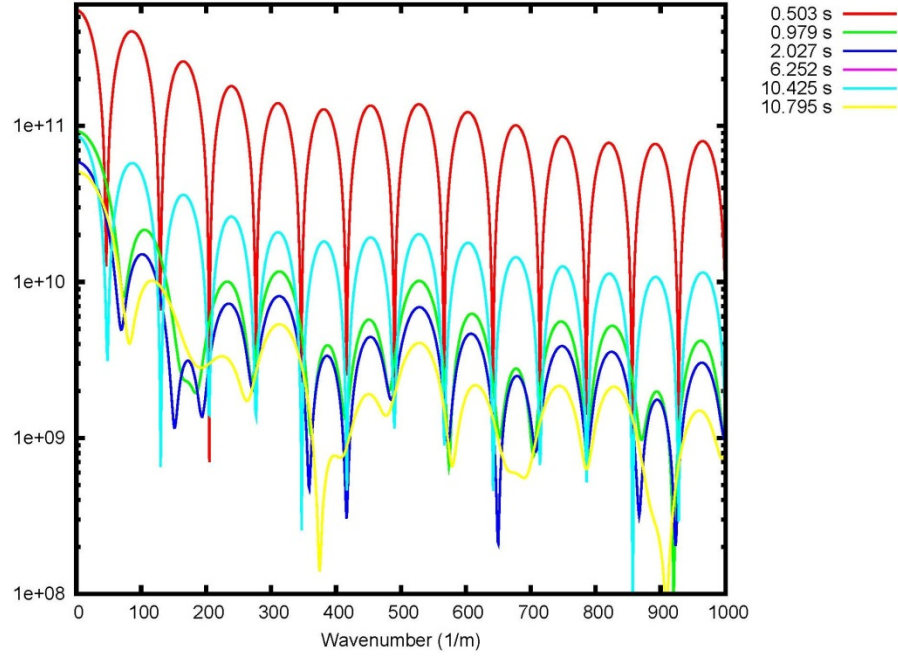
Figure 12. Power spectral wavenumber density for x-directional enstrophy calculated at selected times
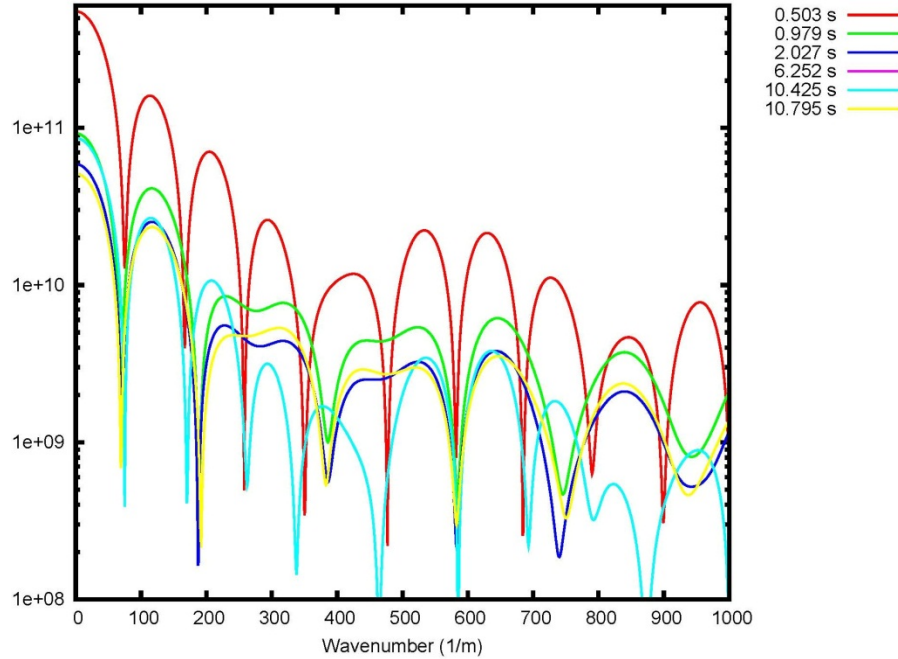
Figure 13. Power spectral wavenumber density for *x*-directional enstrophy calculated at selected times

the RAM for the simulated resins. Also, we can quantify the size of the smallest eddies at about 1.2 cm. Based upon direct observation of RAM tests, this value seems quite reasonable for this early stage. Of course, this mixing scale is insufficient for the mixing of nano-particles, but the solution must be advanced farther in time with increased spatial resolution to examine this mixing scale.

4.0 CONCLUSIONS

Resonant Acoustic Mixing (RAM) is a process that may be used to mix a wide array of materials such as liquids (such as viscous resins), non-Newtonian rheological materials and particles without the use of blades. Of course, rotary blades assemblies are routinely used in high shear mixing, the industrial mixing process most familiar to people everywhere. RAM avoids the use of these blades, so the mixture constituents come into contact only with themselves and the container. This process may ultimately prove to be of interest in combining resins with nano-particles, but we currently do not its effectiveness. Neither the thoroughness of mixing nor the length scales are quantitatively known. The eddy sizes incurred during time-dependent mixing become very important as do eddy interactions with nano-particles. This issue is of great concern since nano-particles are very difficult to handle. This report takes a second small step in studying some of these phenomena.

A previous report by the author addressed the mechanics of modeling RAM by using a modified version of the LESLIE3D multiphase physics code. In this case, simple gas species mixing is discussed along with the results of an attempt at high viscosity mixing. This report studies the latter problem in greater detail. We have simulated the mixing of two high viscosity species (simulated resins) in the RAM. The dynamic viscosities have been scaled in proportion to the actual resins, and we have successfully achieved a numerical model of the mixing process. Moreover, we have developed post-processing techniques to study the mixing process. The motion of eddies in the mixture is analyzed in some detail, and we have developed a technique for measuring the acceleration encountered by a fluid element. This acceleration measurement is output directly by the RAM. Also, the distribution of vorticity has been studied, and we have observed similar behavior in the RAM. We have applied the techniques of Fourier analysis to estimate the length scales for eddies encountered during the mixing process. We can see time dependent change in these scales, and we have identified the minimum eddy size produced during the simulation time interval. This data is shown in the results section of this report. In summary, it seems that resonant acoustic mixing generates a high level of shear without the use of mechanical blades. It also induces a cascade of rotational energy for mixing. This behavior presents advantages for RAM. Further investigation is needed to elucidate a better understanding of the associated physics.

In the future, we plan to incorporate gravity within the simulation since it may have important effects on mixing heavier materials. We also plan to introduce particles into the simulation, first as a diffuse dispersed field within a resin. Later, we will study the mixing of a dense field of particles within a component resin. To support this work, attendant changes are to be made to LESLIE3D, including the use of new equations of state. Comparisons are to be made with experimental data on the thoroughness of mixing. We also plan to extend the size of the simulation for massively parallel execution.

REFERENCES

1. Pope, S.B., *Turbulent Flows*, Cambridge University Press, New York, 2000.

2. Schlicting, H., *Boundary Layer Theory*, 7th Ed., McGraw-Hill, Inc., New York, 1979.

3. ResonantAcoustic$^{®}$ Mixing, Resodyne Acoustic Mixers, Butte, Montana, 2013, pp. 1-8.

4. Meirovitch, L., *Elements of Vibration Analysis*, 2nd Ed., McGraw-Hill, New York, 1975.

5. Richtmyer, R.D., "Taylor instability in shock acceleration of compressible fluids", *Communications in Pure and Applied Mathematics*, Vol. 13, 1960, pp. 297-319.

6. Hirsch, C., *Numerical Computation of Internal and External Flows*, John Wiley & Sons, New York, 1990.

7. Eliezer, S., Ghatak, A. and Hora, H., *Fundamentals of Equations of State*, World Scientific, New Jersey, 2002.

8. Nance, D.V., "Simulating the Resonant Acoustic Mixer", Technical Report, AFRL-RW-EG-2013-079, 2013.

9. MacCormack, R.W., "The effect of viscosity in hypervelocity impact cratering", *Journal of Spacecraft and Rockets*, Vol. 40, No. 5, 2003, pp. 757-763.

10. Menon, S., "Active combustion control in a ramjet using large-eddy simulations", *Combustion Science and Technology*, Vol. 84, 1992, pp. 51-79.

11. Poinsot, T.J. and Lele, S.K., "Boundary conditions for direct simulations of compressible viscous flows", *Journal of Computational Physics*, Vol. 101, 1992, pp. 104-129.

12. Hardin, J.C., *Introduction to Time Series Analysis*, NASA-RP-1145, NASA Langley Research Center, 1986.

13. Rajesh, K.K, "Thrust modulation is a nitrous-oxide/hydroxyl-terminated polybutadiene hybrid rocket motor", AIAA 2006-4503, 42nd AIAA/ASME/SAE/ASEE Joint Propulsion Conference & Exhibit, Sacramento, CA, 2006.

14. Grebowicz, J., Aycock, W. and Wunderlich, B., "Heat capacities of 1,4-polybutadienes", *Polymer*, Vol. 27, 1986, pp. 575-582.

15. Hydroxyl Terminated Polybutadiene Resins and Derivatives – Poly bd and Krasol, Product Bulletin, Sartomer Company, Inc., Exton, PA, 2013.

16. Hardin, J.C., "Regarding numerical considerations for computational aeroacoustics", *Computational Aeroacoustics*, Hardin, J.C. and Hussaini, M.Y., Eds., Springer-Verlag, New York, 1993, pp. 216-228.

LIST OF ACRONYMS, ABBREVIATIONS, AND SYMBOLS

This section contains brief definitions of various terms and acronyms used throughout this document. Only terms and acronyms whose definitions are considered uncommon are included.

C_p - Constant pressure specific heat
C_v - Constant volume specific heat
D_m - Diffusion coefficient for species m
E - Total energy per unit mass
e - Specific internal energy
f - Frequency in Hertz
h_m - Enthalpy of species m
K - Heat conduction coefficient
$k_{x,y,z}$ - Component wavenumbers
P - Thermodynamic pressure (absolute)
q_i - i^{th} component of heat conduction vector (Fourier's Law)
R - Species perfect gas constant
T - Absolute temperature
t - Time coordinate
u_i - i^{th} Cartesian velocity component
V_{im} - i^{th} Cartesian component of diffusion velocity for species m
x_i - i^{th} Cartesian space coordinate
Y_m - Mass fraction of chemical species m

γ - Ratio of specific heats
Δh_{fm}^0 - Heat of formation for species m
δ_{ij} - Dirac delta
λ - Stoke's parameter
μ - Dynamic viscosity
ρ - Mixture density
τ_{ij} - Shear stress tensor
$\vec{\omega}$ - Vorticity vector
$\omega_{x,y,z}$ - Vorticity vector components
$\dot{\omega}_m$ - Production rate for species m

DISTRIBUTION LIST
AFRL-RW-EG-TR-2013-108

Defense Technical Information Center	1 Electronic Copy (1 file, 1 format)
Attn: Acquisition (OCA)	
8725 John J. Kingman Road, Ste 0944	
Ft Belvoir, VA 22060-6218	

EGLIN AFB OFFICES:

AFRL/RWOC (STINFO Tech Library Copy)	1 Copy
AFRL/RW CA-N	Notice of publication only
AFRL/RWMES	1 Copy